DEVELOPMENT OF THE DESIGN GUIDELINES USING CFD TECHNOLOGY FOR A PARTICLES SUSPENSION MIXING TANK

JIMMY LEA AND ADESOJI A. ADESINA*

Abstract — Seven important variables having profound impact on the ability of a mixing tank to suspend particles have been investigated using computational fluid dynamics (CFD) technology. The results obtained from this study can be applied across a broad range of industries such as the chemical, biochemical, petrochemical and mineral processing industries. Finally, a design template incorporating the optimum operating range to suspend particles was developed as a result of this study.

I. INTRODUCTION

In the process industry, suspension of particles denser than its fluid media is one of the most common and important goals. Achieving complete suspension of the particles lead to homogeneous suspension while achieving partial success leads to inhomogeneity and eventually product quality issues. Despite the industrial relevance of this operation, the impact on the performance of the suspension mixing tank through changing several crucial variables has received poor research attention. Moreover, in many instances the design of a mixing tank for suspending particles is based on empiricism and rule-of-thumb. Consequently, such mixing tank or reactor designs lead to sub-optimum process condition which inevitably gives poor product quality consistency and yield. Significant improvements of the design capability and reliability of suspension mixing tank may be expected from advances in computational fluid dynamics (CFD) simulation. In current technology, CFD offers a cost-effective means of capturing the hydrodynamic phenomena and the ability to quantify the performance suspension mixing tank. The purpose of this paper is to therefore to provide a comprehensive coverage of this topic including providing design guidelines, to address the research gap and to equip operation engineers the knowledge to improve their process operation. In addition, the correlations provided in this paper can also be used to estimate the increase or decrease in the power requirement in response to changes made to the mixing tank configuration. The availability of such estimation allows for greater flexibility in process operation.

The authors are with:
Reactor Engineering and Technology Group
School of Chemical Sciences and Engineering,
The University of New South Wales, NSW 2052, Australia
* Corresponding author: a.adesina@unsw.edu.au

II. OBJECTIVES AND KEY PERFORMANCE INDICATOR

A. Objectives

The aims of this paper are to provide a comprehensive coverage of this topic by providing design guidelines and to address the research gap. Specifically, this paper presents a numerical analysis of several key variables with a view to developing suspension mixing tank design guidelines.

B. Key variables

Seven crucial variables known to have a profound effect on the ability of a mixing tank to suspend particles were investigated numerically, namely: baffle width to tank diameter ratio (B/T), baffle spacing to tank diameter ratio (b/T), number of baffle (N_{BF}), impeller rotational speed (N), number of blades (N_B), impeller diameter to tank diameter ratio (D/T) and number of impeller (N_I). Overall, these seven variables constitute the crucial parameters that determine the success of a given geometrical configuration in suspending particles. The geometrical configuration simulated consisted of a standard 6-bladed 45° pitched-blade turbine, 4 standard wall baffles and a spherical-bottom tank.

C. Key Performance Indicator

A horizontal plane across the impeller was created, as shown in Fig. 1, so that surface integration can be conducted to quantify the amount of axial flow passing through the impeller for each trial condition.
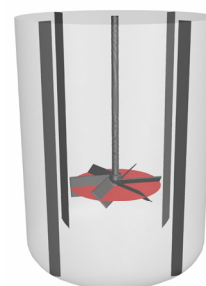

Fig. 1. Key performance indicator

Such an approach enables the determination of the axial flow, minus the radial flow component. The amount of axial flow generated is taken as the key performance indicator (KPI). The reason is because it is the axial flow component that pushes the particles to the tank bottom where they are then deflected by the tank bottom causing the particles to travel in the upward direction. In other words, the cloud height is dependent on the amount of axial flow discharge by the impellers [1-2]. A CFD model validation study was successfully carried out via PIV experiment and the details can be obtained in [3]. The same validated-model was employed for the simulations described in this paper. This ensures the integrity of the results presented.

Integrated values were plotted as a function of each variable and their respective behaviour expressed mathematically. These equations were then differentiated at their turning points to obtain the maximum or minima values.

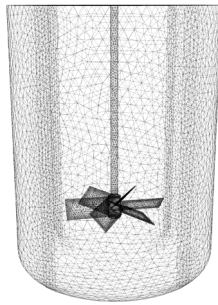### III. THEORETICAL CONSIDERATION

A. Meshed geometry

Fig. 2. Key performance indicator

The meshed geometry of the suspension mixing tank was created using Gambit 2.2.30. It consisted of about 473,810 tetrahedral cells, as shown in Fig. 2. A significantly higher number of cells were allocated to area of high velocity and pressure gradient, notably the rotating zones. The baffles were assumed to have zero thickness in order to eliminate additional meshing within the tank. Meshing baffles with non-zero thickness means that very small cells will be required and this can lead to prohibitively large number of cells with attendant computational costs.

B. Grid independence

A preliminary grid convergence study was carried out to verify that the solution obtained from using the second-order upwind discretisation scheme was mesh independent. The number of cells inside and outside the rotational zones was systematically increased in the x-, y- and z-directions throughout the tank. When refining the mesh, care was taken to assign additional cells to the regions of high gradient around the impeller blades and discharge regions. Simulation results did not show significant changes (<1%) when the number of cells was increased.

C. Numerical setup

Fluent 6.2.16 solver was used to create a numerical solution that matches the governing conservation equations. In this study, the focus was on solving the conservation of mass, momentum and turbulence transport with a view to generating a steady-state 3D hydrodynamics profile. The conversation of mass is given as:

$$\frac{\partial \rho}{\partial t} = -(\nabla \cdot \rho \upsilon) \qquad (1)$$

where $\partial \rho / \partial t$ is rate of increase of mass per unit volume and $-(\nabla \cdot \rho \upsilon)$ is the net rate of mass addition per unit volume by convection. The conversation of momentum is given as:

$$\frac{\partial \rho \upsilon}{\partial t} = -(\nabla \cdot \rho \upsilon \upsilon) - \nabla p - (\nabla \cdot \tau) + \rho g \qquad (2)$$

where $\partial \rho \upsilon / \partial t$ is rate of increase of momentum per unit volume, $-(\nabla \cdot \rho \upsilon \upsilon)$ is the rate of momentum addition by convection per unit volume, $-\nabla p - (\nabla \cdot \tau)$ is the rate of momentum addition by molecular transport per unit volume and ρg is the external force on fluid per unit volume. For constant ρ and μ, insertion of the Newtonian law of viscosity for τ into (2) leads to:

$$\rho \frac{D\upsilon}{Dt} = -\nabla p + \mu \nabla^2 \upsilon + \rho g \qquad (3)$$

Equation (3), famously known as the Navier-Stokes equation, provides the usual starting point for the analysis of flow processes. The finite volume (FV) method uses the integral form of the conservation of equations as its starting point to ensure global conservation. Differential equation is integrated over the volume of each cell to obtain algebraic equations.

To simulate impeller rotations, separate rotational zones in the immediate vicinity of the impellers were created and a multiple reference frame (MRF) approach was employed. This method involved solving the flow characteristics of the inner region using a rotating framework. These results were then used to provide boundary conditions for the outer region which employs a stationary framework to secure solution to the flow characteristics. The results from the outer region were then re-supplied as boundary conditions for the inner region. This iterative procedure was repeatedly

performed until a convergent solution was obtained for both regions.

The segregated-implicit method, where the governing equations were solved sequentially was used. To obtain a higher degree of accuracy, all solutions were obtained via the second-order upwind scheme. In this scheme, higher order accuracy was obtained at the cell surfaces whereby the values at the cell centroid were subjected to multidimensional linear reconstruction using the Taylor series expansion, as shown in (4) and (5).

$$f(x) = f(x_0) + \frac{1}{1!} f'(x_0)(x - x_0)$$
$$+ \frac{1}{2!} f''(x_0)(x - x_0)^2 + ...$$
$$+ \frac{1}{n!} f^n(x_0)(x - x_0)^n + R^{n+1}$$
(4)

where

$$R^{n+1} = \frac{1}{(n+1)!} f^{(n+1)}(\xi)(x - x_0)^{n+1}$$
(5)

Due to the presence of baffles, significant interrupted rotational flow existed inside the mixing unit thus creating steep pressure gradient. As a result, PRESTO (pressure staggering option) was employed to compute the pressure value at the cell surface by interpolating the values at the cell centroid. The lack of solid body rotation justifies the use of the Realizable k-ε model to capture the hydrodynamic phenomenon. The kinetic energy can be represented by:

$$\frac{\partial}{\partial t}(\rho k) + \frac{\partial}{\partial x_j}(\rho k u_j) = -\frac{\partial}{\partial x_i}\left[(\mu + \frac{u_t}{\sigma_k})\frac{\partial k}{\partial x_j}\right]$$
$$+ G_k + G_b - \rho\varepsilon - Y_M + S_k$$
(6)

and the dissipation rate is represented by:

$$\frac{\partial}{\partial t}(\rho\varepsilon) + \frac{\partial}{\partial x_j}(\rho\varepsilon u_j) = \frac{\partial}{\partial x_j}\left[(\mu + \frac{u_t}{\sigma_\varepsilon})\frac{\partial \varepsilon}{\partial x_j}\right] +$$
$$\rho C_1 S_\varepsilon - \rho C_2 \frac{\varepsilon^2}{k + \sqrt{v\varepsilon}} + C_{1\varepsilon}\frac{\varepsilon}{k}C_{3\varepsilon}G_b + S_\varepsilon$$
(7)

where

$$C_1 = \max\left[0.43, \frac{\eta}{\eta + 5}\right]$$
(8)

$$\eta = S\frac{k}{\varepsilon}$$
(9)

$$S = \sqrt{2S_{ij}S_{ij}}$$
(10)

In equations (6) and (7), G_k represents the turbulence kinetic energy generated due to the mean velocity gradients whereas G_b is the turbulence kinetic energy due to buoyancy. Y_M represents the contribution of the fluctuating dilation in compressible turbulence to the overall dissipation rate. C_2 and $C_{1\varepsilon}$ are constants while σ_k and σ_ε are the turbulent Prandtl numbers for k and ε respectively.

D. Convergence criteria

Simulations were generally considered converged when the residuals for mass, momentum and turbulence k-ε, fell below 1×10^{-4}. Further checks for convergence were made by creating a monitoring point inside the tank and ensuring that the value monitored remained constant with further iterations.

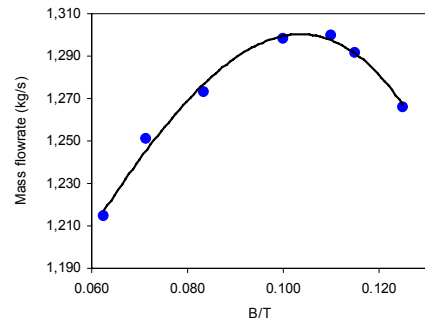### IV. RESULTS AND DISCUSSIONS

A. B/T

Fig. 3. Mass flowrate vs baffled width to tank diameter ratio

Fig. 3 shows the relationship between the mass flowrate and the impeller diameter to tank diameter ratio. Its behaviour is governed by a third-order polynomial expression, having a good correlation coefficient, R=0.9899. The expression is given by:

$$\dot{m} = -380882\left(\frac{B}{T}\right)^3 + 53465\left(\frac{B}{T}\right)^2 + 1189\left(\frac{B}{T}\right) + 1027$$
(11)

For optimum performance, $\left(\frac{B}{T}\right) = 0.1036$

The purpose of baffles is to convert radial flow into axial flow. The maximum value is at $B/T = 0.1036$, which explains why most baffles in the industry have widths ranging from 1/12 to 1/10 because beyond 1/10, the mass

flowrate would drop. When the baffle widths were too small, the flow resistance was small which means the amount of radial flow converted to axial flow was minimal. An increase in the conversion can be achieved by widening the baffle width since doing so will increase the amount of flow resistance. But as the baffle width were further widened, too much flow resistance was provided by the baffles to such extent that not much radial flow was there to be converted to axial flow. As a consequence, beyond B/T=0.1036, the mass flow rate started to drop. From here it can be seen that for standard wall baffles, the optimum B/T ratio is 1/10.
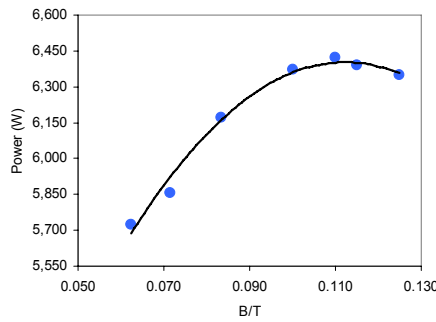
Fig. 4. Power consumption vs baffle width to tank diameter ratio

Fig. 4 shows the power consumption as a function of the baffle width, and this is described by the polynomial model:

$$P = -288907\left(\frac{B}{T}\right)^2 + 64864\left(\frac{B}{T}\right) + 2762 \qquad (12)$$

with R = 0.9872. From (12), increasing B/T value from 0.063 to 0.10 (58.73%) will increase the power consumption by 369.6%. Increasing the B/T value from 0.10 to 0.15 (50%) will cause a reduction in the flowrate by 44.07%.
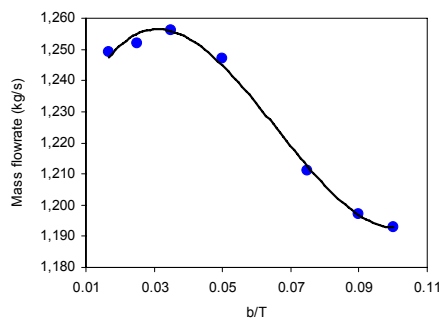
B. b/T

Fig. 5. Mass flowrate vs baffled spacing to tank diameter ratio

Fig. 5 shows the relationship between the mass flowrate and the impeller diameter to tank diameter ratio and is governed by the following fourth-order polynomial expression with good regression of 0.9961:

$$\dot{m} = 376766\left(\frac{b}{T}\right)^3 - 74426\left(\frac{b}{T}\right)^2 + 3529\left(\frac{b}{T}\right) + 1207 \qquad (13)$$

The maximum value is at b/T = 0.031

From the maximum value, baffle clearance produced peak mass flowrate at 1/32 (b/T=0.031). At small b/T value, the baffles were located rather far way from the impellers and therefore did not contribute significantly to the flow resistance. This means that not much radial flow was converted to axial flow. As the clearance widened, the baffles were closer to the impellers thereby converting most of the radial flow to axial flow. This automatically maximised the mass flowrate in the axial direction.

However, as the clearance was further widened, the flow resistance dropped because the clearance was large enough for the fluid to flow pass behind the baffles with minimal interruption. This means that placing the baffles too far away from the tank wall will cause a reduction in the axial flowrate because the baffles do not convert enough radially oriented flow to axially oriented flow.
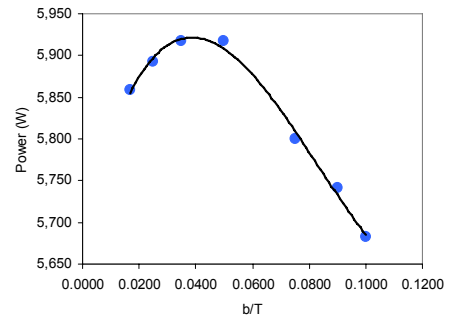

Fig. 6. Power consumption vs baffled spacing to tank diameter ratio

Fig. 6 shows the power consumption as a function of various values of b/T expressed with a good regression of 0.9942 as:

$$P = 884245\left(\frac{b}{T}\right)^3 - 219838\left(\frac{b}{T}\right)^2 + 13047\left(\frac{b}{T}\right) + 5695 \qquad (14)$$

The peak power consumption occurred at b/T = 0.03872

The power increase from 1/60 to 1/30 and beyond this b/T value, the power consumption started to decrease. At small b/T value, the baffle presented negligible resistance to flow. As the spacing widened, the baffles were closer to the impellers therefore contributing more flow resistance. However, as the spacing was further widened, the flow resistance dropped because the spacing was large enough for the fluid to flow pass behind the baffles with minimal interruption. This phenomenon caused a reduction in the power consumption.
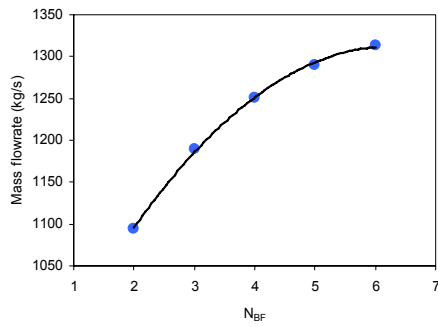
C. N_{BF}

Fig. 7. Mass flowrate vs number of baffle

Fig. 7 shows the relationship between the mass flowrate and number of baffles, which is governed by the following quadratic polynomial expression with good regression of 0.9991:

$$\dot{m} = -11.93 N_{BF}^2 + 149.3 N_{BF} + 844.8 \qquad (15)$$

Using (15), increasing the number of baffles from 2-3, 3-4, 4-5 and 5-6 resulted in an increase in axial flowrate by 8.120%, 5.570%, 3.357% and 1.392% respectively.
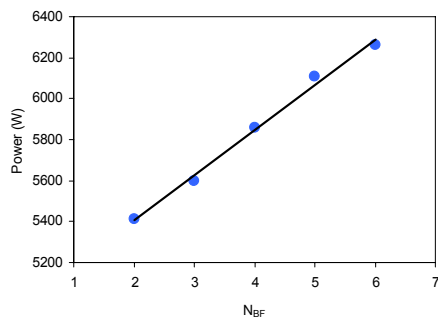

Fig. 8. Power consuption vs number of baffle

Fig. 8 shows the power consumption as a function of the number of baffles can be represented by a linear function with regression of 0.9928 with the form:

$$P = 220.42 N_{BF} + 4967 \qquad (16)$$

From (16), the power consumption will increase by 4.076% for every baffle installed in the system.
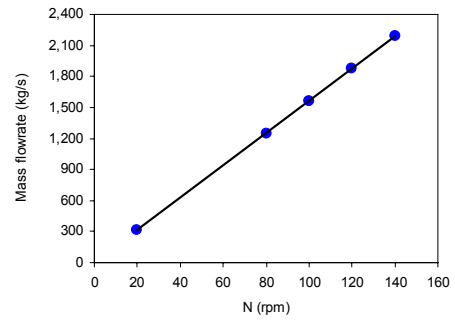
D. N

Fig. 9. Mass flowrate vs N

Fig. 9 shows that the flowrate increased by increasing the impeller rotational speed, which follows a linear relationship, with regression of 1. It can be expressed as:

$$\dot{m} = 15.65 N \qquad (17)$$

From (17), an increase in the speed by 1% results in 1% increase in the axial mass flowrate. The recommended impeller rotational speed is any speed that is much greater than the just suspended speed, N_{js}. N_{js} is defined as the minimum rotational speed required to lift the particles from the tank bottom and that no particles remain on the tank bottom for any longer than 1-2 seconds. N_{js} can be obtained via the Zwietering correlation [4], which is given as:

$$N_{js} = S v^{0.1} \left[\frac{g(\rho_s - \rho_l)}{\rho_l} \right]^{0.45} X^{0.13} d_p^{0.2} D^{-0.85} \qquad (18)$$

where:

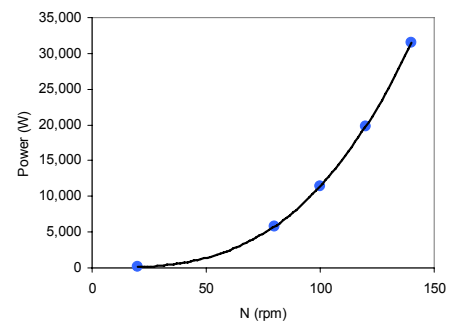|		
S = Zwietering constant	-	
v = kinematic viscosity	$m^2 s^{-1}$	
g = gravitational constant	$m s^{-2}$	
ρ_s = density of solid media	$kg m^{-3}$	
ρ_l = density of liquid media	$kg m^{-3}$	
X = solid loading	-	
d_p = diameter of solid particles	m	
D = impeller diameter	m	

Fig. 10. Power consumed vs N

Fig. 10 shows that the power consumption relationship with the impeller rotational speed followed a power function with a regression of 1. It can be expressed as:

$$P = 0.0103(N)^{3.0222} \qquad (19)$$

Based on eqn (19), increasing the speed by 300% from 20rpm to 80rpm will increase the power consumption by 5,812%, that is, a 1% increase in the speed in this range will increase the power consumption by 19.37%. Increasing the speed from 80rpm to 140rpm (75%) will increase the power consumption by 442.7%. Therefore for every percent increase in the speed, the power consumed will be increase by 5.902%.

E. N_B
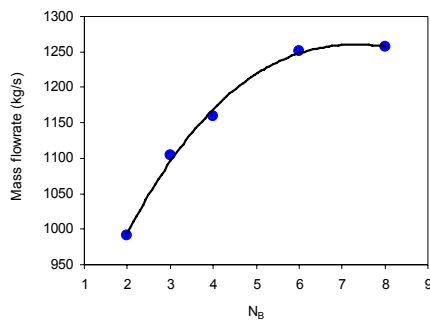
Fig. 11 Mass flowrate vs number of blades

Fig. 11 shows the relationship between the mass flowrate and the impeller diameter to tank diameter ratio and is governed by the following model,

$$\dot{m} = \frac{aN_B}{1 + bN_B} \qquad (20)$$

where $\dot{m}$ represents mass flowrate and N_B represents the number of blades. Data regression to (17) yielded a=1667 and b=1.167 with an excellent correlation fit of 0.9992. The increase in mass flowrate when the number of blades was increased from 2 to 3 blades was 11%, from 3 to 4 blades was 5.851%, from 4 to 6 was 6.287% and from 6 to 8 blades was 3.2%. Increasing the number of blades from 6 to 8 did not return a significantly higher mass flowrate value. From a practical standpoint, a 6-bladed impeller is recommended.
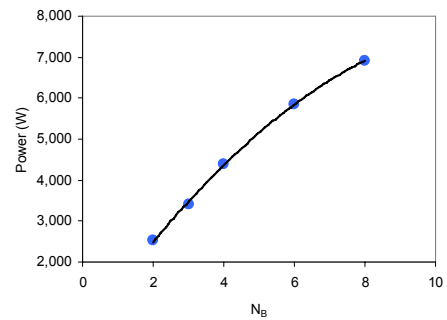

Fig. 12. Power consumed in Watts vs N_B

Fig. 12 shows that the power consumption as a function of the number of blades followed a quadratic polynomial function with a good regression of 0.9994, which can be expressed as:

$$P = -50.07(N_B)^2 + 1241(N_B) + 201.9 \qquad (21)$$

Referring to (21), increasing the blades from 4 to 6 will increase the power consumption by 33.91% and 18.48% from 6 to 8 blades.
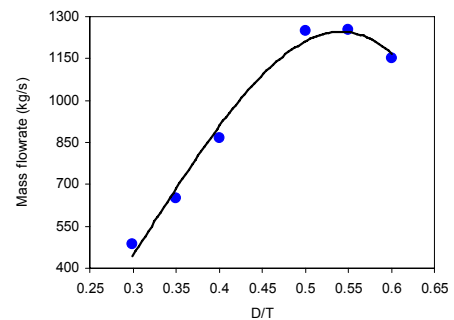
F. D/T

Fig. 13. Mass flowrate vs D/T

Fig. 13 shows the relationship between the mass flowrate and the impeller diameter to tank diameter ratio and is governed by the following third-order polynomial expression,

$$\dot{m} = -31491\left(\frac{D}{T}\right)^3 + 29886\left(\frac{D}{T}\right)^2 - 4648\left(\frac{D}{T}\right) \qquad (22)$$

with a good regression value of 0.9875. Simple differentiation at the turning point shows that the maximum value is located at $D/T = 0.54$.

From (22), increasing the ratio from D/T=0.3 to D/T=0.54 increased the mass flowrate however, increasing the D/T value beyond the maximum value will caused a reduction in

the mass flowrate. From D/T=0.3 to D/T=0.4 (33% increment), the increase in mass flowrate was 104%, from D/T=0.4 to D/T=0.55 (37.50% increment), the increased was 37.25% and from D/T=0.55 to D/T=0.6 (9.09% increment), the reduction in flowrate was 6.265%.

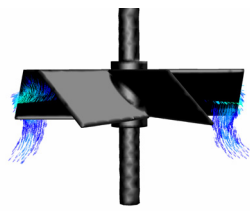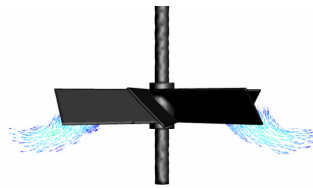For optimum performance: $0.5 \leq D/T \leq 0.55$.

Fig. 14. D/T=0.4   Fig. 15. D/T=0.55

The reduction in the mass flowrate when the D/T ratio was increased to value beyond the maximum value may be attributed to the change in the flow profile discharged by the impellers. Fig. 14 shows that at D/T=0.4, the flow discharge was axial in nature but when D/T=0.55, the flow changed from axial flow to radial flow as shown by the vector plot in Fig. 15. Obviously, the amount of fluid that passed through the horizontal plane decreased per unit time.
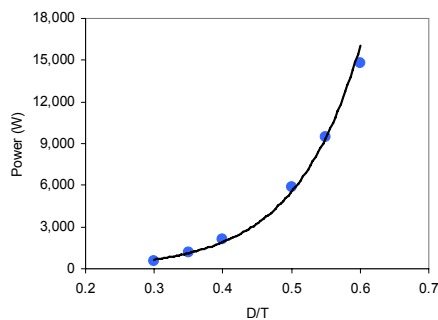
Fig. 16. Power consumed in Watts vs D/T

Fig. 16 shows that the power consumed when D/T was increased from 0.3 to 0.6 follows an exponential relationship with a good regression of 0.9956 in the form:

$$P = 27.19e^{10.63\left(\frac{D}{T}\right)} \quad (23)$$

From (23), when D/T was increased from D/T=0.3 to D/T=0.4, the increased in power consumption was 190%, from D/T=0.4 to D/T=0.55, the increased power consumption was 393% and from D/T=0.55 to D/T=0.6, the increased in power consumption was 70.15%.

The huge increase in the power consumption between D/T=0.4 to D/T=0.55 reflects the high increase in the flowrate. Although the power consumption is higher in this D/T range, it is required to achieve process objective.
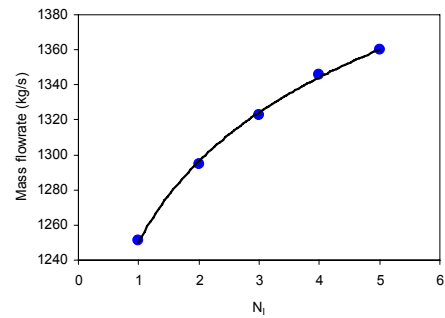
G. N_I

Fig. 17. Mass flowrate vs N_I

Fig. 17 shows the relationship between the axial mass flowrate and the number of impeller installed on the same shaft can be expressed as:

$$\dot{m} = 1250N_I^{0.0524} \quad (24)$$

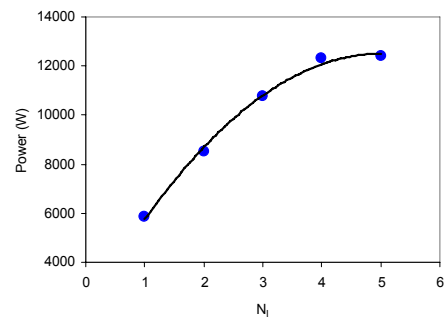with a correlation coefficient of 0.9991.

Fig. 18. Power consumed vs flowrate vs N_I

Fig. 18 shows the relationship between the power consumed by the process and the number of impeller installed on the same shaft can be expressed as a quadratic function in the form:

$$P = -415.5N_I^2 + 4181N_I + 1991 \quad (25)$$

The percentage increment in the power consumed as a function of the increment in the number of impeller is best represented by the bar chart as shown in Fig. 19.
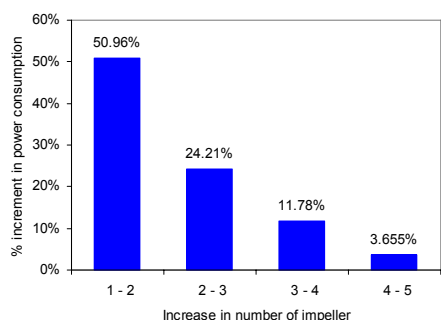
Fig. 19. % increment in power consumption vs increase in N_I

For $Z/T \leq 1.4$, $N_I = 2$ since beyond this number, the increase in the flow rate did not warrant the increase in the power consumption.
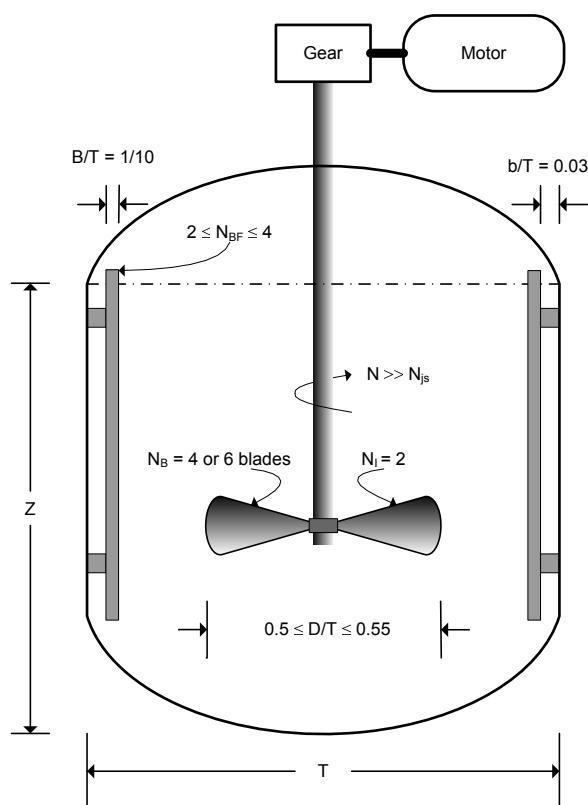
V. SUMMARY OF OPTIMUM OPERATING RANGE

Fig. 20. Design template

The summary of the optimum operating range for each variable can be best represented by a design template shown in Fig. 20, where Z and T denote liquid height and tank diameter respectively. This template provides a convenient means of optiming a suspension mixing tank without having to conduct time-consuming physical experiments and provides the user a direct route to optimisation. It must be noted however, this design template is only applicable to a contemporary design suspension mixing tank or mixing tank where the geometrical configuration resembles that provided in Fig. 20. The information in this design template can also be used to update current literature on suspension mixing tank.

VI. CONCLUSION

The behaviour of six variables having profound impact on the ability of a mixing tank to suspend particles has been investigated. The behaviour of each variable was adequately described by a polynomial model. The underlying reasons responsible for the behaviour of each variable under investigation was also provided. Results show that out of the six variables investigated, four variables have operating range where performance is at its optimum. A design template that summarises the results was provided as a design guideline.

REFERENCES

[1] Lea J and Adesina A [2006], Simulation of the mixing tank for the production of military high explosive RDX/TNT − A computational fluid dynamics approach, *CHEMECA*, September 17-20 2006, Auckland, New Zealand.

[2] Lea J and Adesina A [2006], Analysis of the mixing tank for cyclotol production: A CFD simulation study, *APCCHE* Aug 27-30 2006, Kuala Lumpur, Malaysia.

[3] Lea J, Gehrig A, Flavel P and Adesina A [2005], The CFD modelling and simulation of nitration unit employed for the manufacture of military propellant, *ICCHMT* May 17-20 2005, Paris, France.

[4] Zwietering T.N. [1958], Suspending of solid particles in liquid by agitators, *Chemical Engineering Science*, Vol 8, 244-253.